

# Microstructure of laser-clad SiC–(Ni alloy) composite coating

Y.T. Pei, J.H. Ouyang, T.C. Lei, Y. Zhou

*Department of Metals and Technology, PO Box 433, Harbin Institute of Technology, Harbin 150001,  
People's Republic of China*

Received 17 May 1994; in revised form 9 August 1994

## Abstract

The laser cladding technique was used to produce Ni alloy coatings with different SiC particle ( $\text{SiC}_p$ ) contents on steel 1045. The complete dissolution of  $\text{SiC}_p$  took place during laser melting and led to a microstructural evolution of the coatings associated with the  $\text{SiC}_p$  content.  $\text{M}_7\text{X}_3$  or  $\text{M}_{23}\text{X}_6$ -type carboborides and Ni-base solid solution are found as the main microstructural constituents of the clad layers, and the volume fraction of the carboborides increases with increasing  $\text{SiC}_p$  content. When the  $\text{SiC}_p$  content reaches 30 vol.%, a silicide of  $\text{Ni}_3\text{Si}_2$  phase and a few spherical graphite precipitates are observed, and the  $\gamma$  matrix shows a modulated structure. The addition of  $\text{SiC}_p$  can significantly enhance the microhardness and wear resistance of the coatings.

**Keywords:** Silicon; Carbon; Nickel; Alloys; Composites

## 1. Introduction

Laser cladding has been developed as a method for producing coatings to enhance the surface resistance of materials against wear, corrosion, erosion and high temperature oxidation. Compared with other surface modification methods, it can offer some unique advantages such as fine microstructure, minimal clad dilution and good fusion bonding. Earlier studies [1–3] were carried out by injecting carbide particles into the laser molten pool to produce carbide-reinforced composite coatings. Abboud and West [4,5] reported some valuable results on injecting coarse SiC particles ( $\text{SiC}_p$ ) into the laser molten pool of commercial purity Ti or Ti–6wt.%Al–4wt.%V alloy. In their investigations, the partial dissolution of  $\text{SiC}_p$  led to matrix enrichment with Si and C so that, during solidification, TiC dendrites precipitated at the particle–matrix interfaces or within the matrix. Abbas and West [6] investigated a laser-clad stellite–SiC composite coating on En3b grade steel and found that the SiC addition led to an increase in the Vickers microhardness from 540–580 HV for the stellite 6 coating without SiC to 1190 HV for the matrix region of the stellite–SiC composite coating and thus to an approximately twofold increase

in wear resistance. They considered that the enhanced hardness and wear resistance were attributed mainly to the enrichment of the stellite in carbon by partial dissolution of  $\text{SiC}_p$  rather than to the presence of undissolved  $\text{SiC}_p$ . Therefore the mechanism of the effect of carbide reinforcement of the coatings on wear properties is not very clear and needs further study. In the present work, a mixture of fine  $\text{SiC}_p$  plus Ni alloy powder was used as clad material in order to study the effect of the  $\text{SiC}_p$  addition on the microstructure and wear behavior of the composite coatings.

## 2. Experimental details

The 40 mm × 20 mm × 10 mm strips of commercial steel 1045 were used as the substrate and a mixture of  $\text{SiC}_p$  and Ni alloy powders was used as the clad material. The volume fraction of  $\text{SiC}_p$  was in the range 5–60 vol.%. The average size of clad powders was 3  $\mu\text{m}$  and 50  $\mu\text{m}$  for SiC and Ni alloy respectively. The normal composition of Ni alloy powder was Ni–15.0wt.%Cr–4.0wt.%B–5.8wt.%Si–0.73wt.%C–12.3wt.%Fe. The thickness of the pre-placed mixture on the substrate was about 0.6 mm.

A 2 kW continuous-wave CO<sub>2</sub> laser was employed to make a series of coating tracks under the conditions of 1000 W laser power, 4 mm s<sup>-1</sup> traverse speed and 3 mm beam diameter. Argon was blown to shroud the molten pool from outside atmosphere.

Transverse sections of the cladding were cut for microstructural studies. Electrolytic etching with a 10 N NaOH solution was used for preparing metallographic specimens. The microstructure of the cladding was analyzed using a Hitachi S570 scanning electron microscope and a Philips CM12 transmission electron microscope. Foils for transmission electron microscopy (TEM) observations were prepared using the ion beam thinning technique. The phases present in the clads were identified using a D/MAX-RB X-ray diffractometer with Cu K $\alpha$  radiation.

Wear tests were carried out without lubrication at room temperature using a pin-on-ring friction-and-wear-testing machine. The ring of the wear couple was made of WC-8wt.%Co hard alloy with a Rothwell A hardness of 89 HRA. The wear conditions were given as 90 N normal load, 1.47 m s<sup>-1</sup> sliding speed and 90–300 m sliding distance.

### 3. Results and discussion

#### 3.1. Phase analysis

The X-ray diffraction (XRD) spectra of the initial SiC powder and the laser-clad coatings are shown in Fig. 1. After laser processing, no SiC characteristic peaks can be detected within all coatings made from Ni alloy and SiC<sub>p</sub> in different proportions. The XRD data

reveal that the SiC<sub>p</sub> has completely dissolved during laser melting and the resolidified coatings consist mainly of Ni-based solid solution and M<sub>7</sub>C<sub>3</sub> or M<sub>23</sub>C<sub>6</sub> in which some carbon atoms are replaced by boron atoms as shown by ion microprobe mass analysis. With increasing SiC<sub>p</sub> content, more and more M<sub>23</sub>X<sub>6</sub> (M $\equiv$ Cr or Fe; X $\equiv$ C or B) and Ni<sub>3</sub>Si<sub>2</sub> compounds formed within the clad layers, and their diffraction peaks became obvious.

#### 3.2. Microstructure of the coatings

Microstructural characteristics of the laser-clad coatings are shown in Fig. 2. Three distinct regions can be clearly found on the cross-section of all coatings: the clad layer labelled CL, transition zone labelled TZ and the heat-affected zone labelled HAZ. In all coatings used in this study the transition zones have a thickness of about 40  $\mu$ m and exhibit a typical eutectic or eutectic-plus-dendritic microstructure, and the eutectics become finer with increasing SiC<sub>p</sub> content. The SiC-free Ni alloy clad layer consists of  $\gamma$ -Ni solid solution and precipitated equiaxed (Cr,Fe)<sub>7</sub>(C,B)<sub>3</sub> particles (Fig. 2(a)). However, the carboboride phases in the 10vol.%SiC-Ni alloy clad layer (Fig. 2(c)) are mostly shaped like a fine column and interpreted as (Cr<sub>0.7</sub>, Fe<sub>0.3</sub>)<sub>23</sub>(C,B)<sub>6</sub> according to the energy-dispersive X-ray analysis (EDXA) and XRD data. The 30vol.%SiC-Ni alloy clad layer (Fig. 2(e)) is characterized by a lamellar eutectic which consists mainly of (Cr<sub>0.7</sub>, Fe<sub>0.3</sub>)<sub>23</sub>(C,B)<sub>6</sub> needles and a  $\gamma$ -Ni matrix in which very fine Ni<sub>3</sub>Si<sub>2</sub> particles precipitate. Microstructural analysis indicates that the volume fraction of carboborides and silicides in the coatings increases significantly with the addition of SiC<sub>p</sub>.

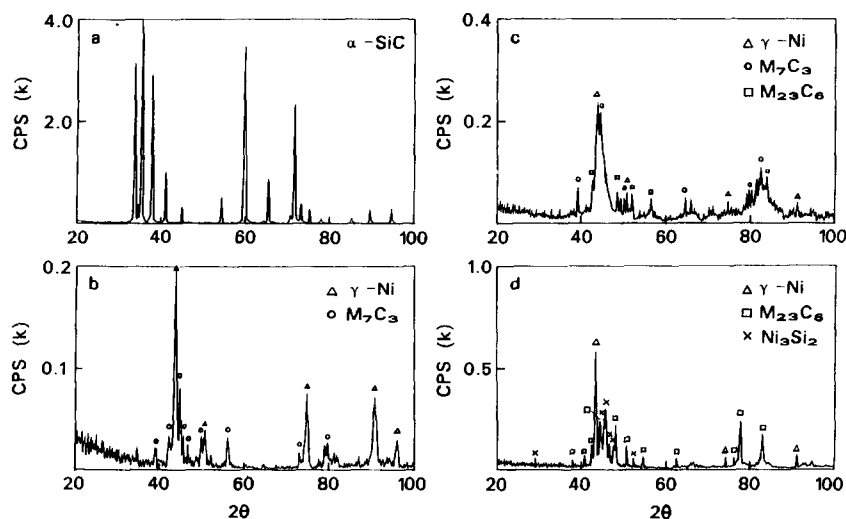


Fig. 1. XRD spectra: (a) the initial SiC powder; (b) single Ni alloy coating; (c) 10vol.%SiC-Ni alloy coating; (d) 30vol.%SiC-Ni alloy coating.

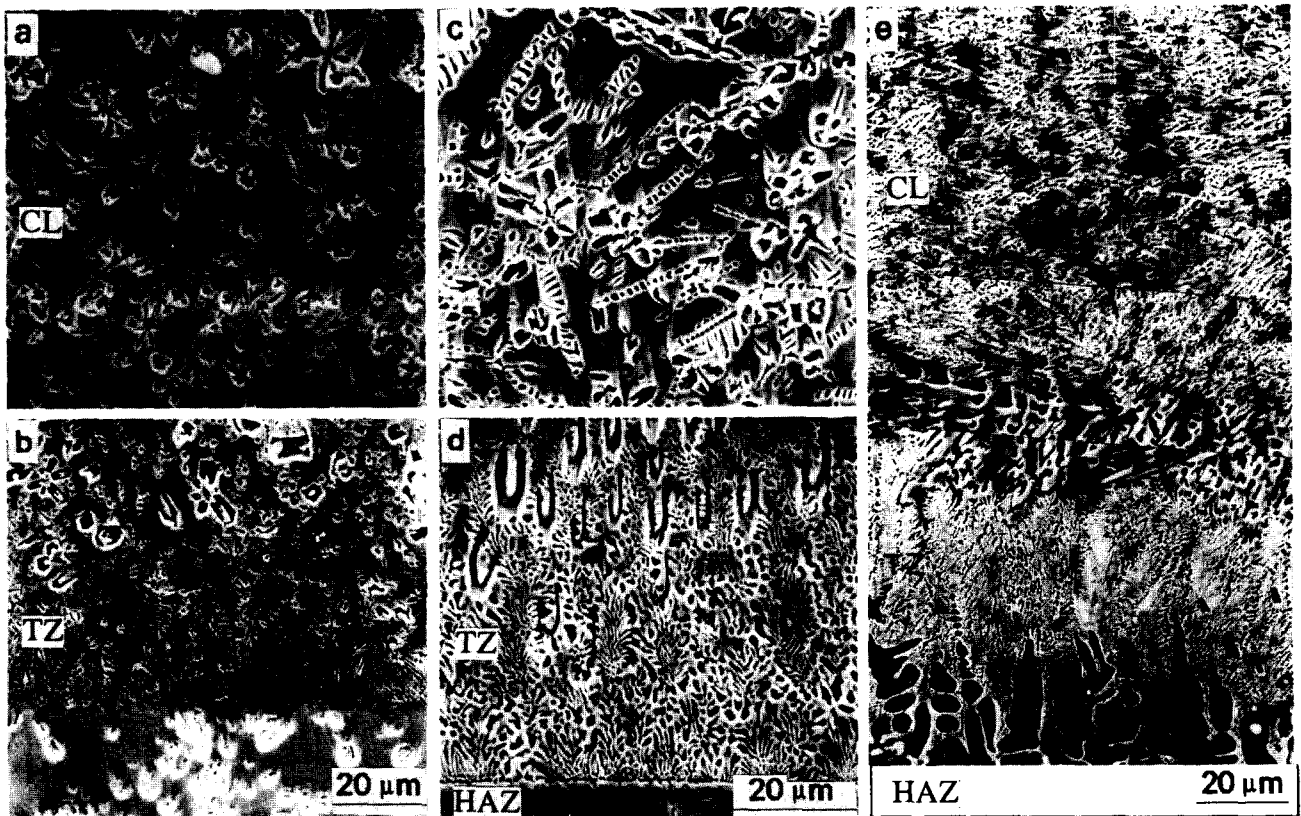
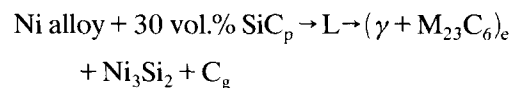
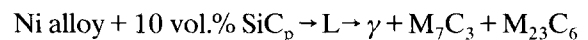
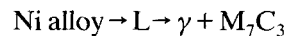


Fig. 2. Microstructure of laser-clad coatings (SEM): (a), (b) Ni alloy without SiC; (c), (d) 10 vol.% SiC–Ni alloy; (e) 30 vol.% SiC–Ni alloy.

The TEM photographs shown in Fig. 3 clearly present the morphology of eutectic carboborides within the clad layers. The higher the SiC<sub>p</sub> content in the initial powder mixture, the finer the carboborides and the closer the contiguity of these hard phases will be. When the SiC<sub>p</sub> content reaches 30 vol.%, some substantial changes take place in the microstructural characteristics of the cladding. The  $\gamma$ -Ni matrix shows a marked tweed contrast in bright field (Figs. 3(c) and 4), and its composition revealed by EDXA is: 41.7 at.% Ni–38.5 at.% Fe–0.9 at.% Cr–18.9 at.% Si. This contrast anomaly may be considered as a typical feature of modulated structure and is very similar to that observed in an Ni–Cu–Si alloy system [7]. This modulated structure can serve as a precursor of, for example, silicide precipitation because there is some supersaturation of Si in the  $\gamma$  phase. In fact, a dark Si-rich phase can be found in Fig. 4 and is interpreted as  $(\text{Ni}_{0.6}, \text{Fe}_{0.4})_3\text{Si}_2$  according to the EDXA results. In addition, a few spherical graphite precipitates can be observed with a substructure of arbitrarily oriented microtwins (Fig. 5). These graphite precipitates nucleated at Al-rich impurities and grew by a twinning mechanism, and the quantity of them increases with further increasing SiC<sub>p</sub> content beyond 30 vol.%.

According to the above analysis, all phases presented in each coating can be summarized into the following reactions:



where L indicates the liquid phase produced by laser irradiation, and the subscripts e and g represent eutectic and graphite respectively.

### 3.3 Microhardness distribution

The distribution of microhardness shown in Fig. 6 indicates three distinctly separated levels which are in good agreement with the three regions of the clad coatings. Obviously, the addition of SiC<sub>p</sub> enhances the microhardness of the coatings. The increase in microhardness is attributed essentially to the dissolution of SiC<sub>p</sub> in the liquid and the consequent increase in the volume fraction of carboborides formed on resolidification. Fig. 7 shows the relationship between the

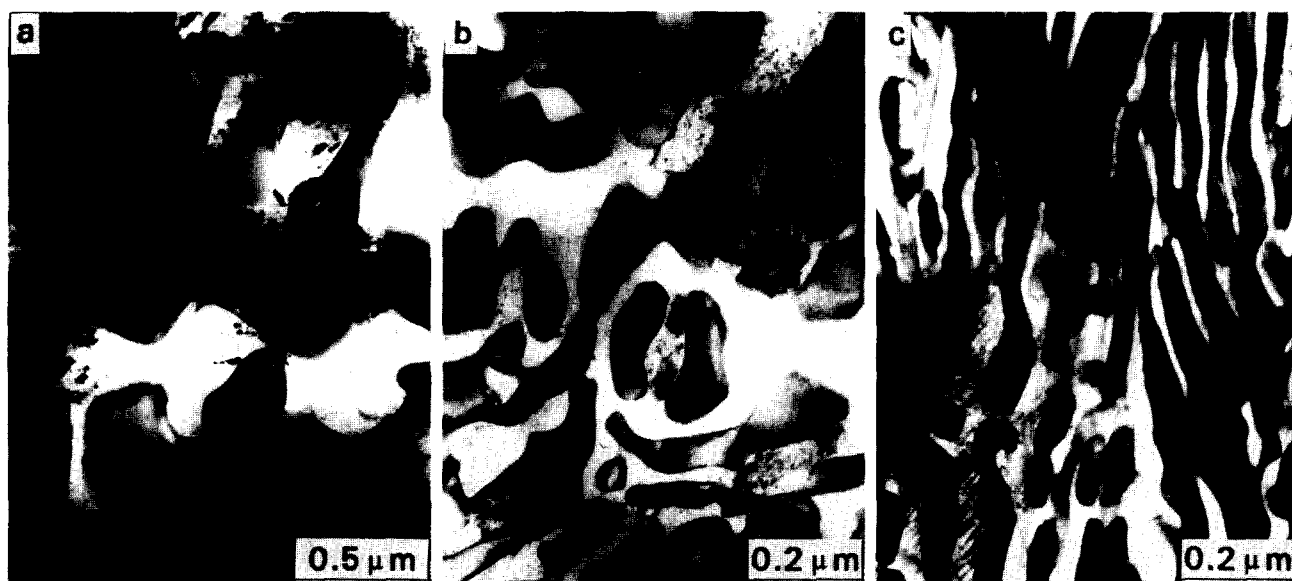
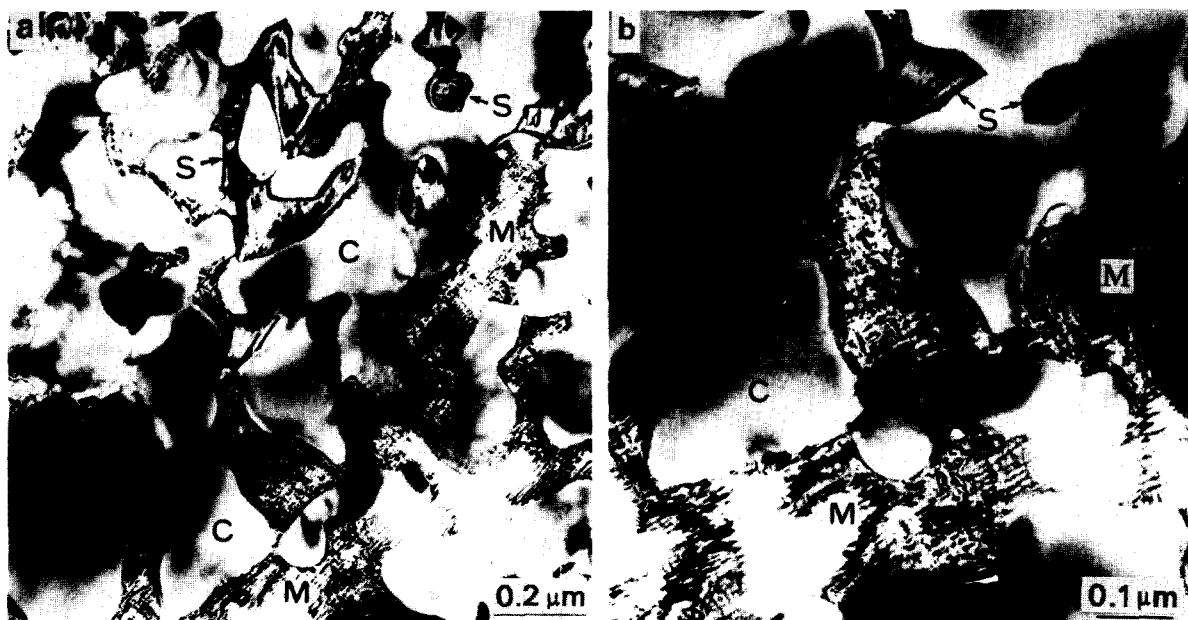


Fig. 3. Morphology of eutectic carboborides within the clad layers (TEM): (a) Ni alloy without SiC; (b) 10vol.%SiC-Ni alloy; (c) 30vol.%SiC-Ni alloy.



marked *M*=Matrix, *C*=Carboboride, *S*=Silicide

Fig. 4. TEM images showing the modulated structure in the matrix (30vol.%SiC-Ni alloy): (a) bright-field image; (b) magnified image.

microhardness and the  $\text{SiC}_p$  content. The Vickers microhardness of the clad layers has a maximum value of 1120 HV at 10 vol.%  $\text{SiC}_p$  content and decreases with further increasing  $\text{SiC}_p$  content beyond 20 vol.%. This change is related to the formation of more  $\text{M}_{23}\text{X}_6$  but fewer  $\text{M}_7\text{X}_3$  carboborides and of the graphite precipitates within the matrix on solidification. In general,  $\text{M}_{23}\text{X}_6$  is not so hard as  $\text{M}_7\text{X}_3$ .

### 3.4. Wear resistance of the coatings

The wear volume of SiC-free Ni alloy and SiC-Ni alloy coatings is given in Fig. 8 which indicates a greatly improved wear resistance caused by the addition of  $\text{SiC}_p$  to the clad layer. A minimum wear volume (about a third of the value of SiC-free Ni alloy) is obtained at 30 vol.%  $\text{SiC}_p$  content. The wear volume decreases

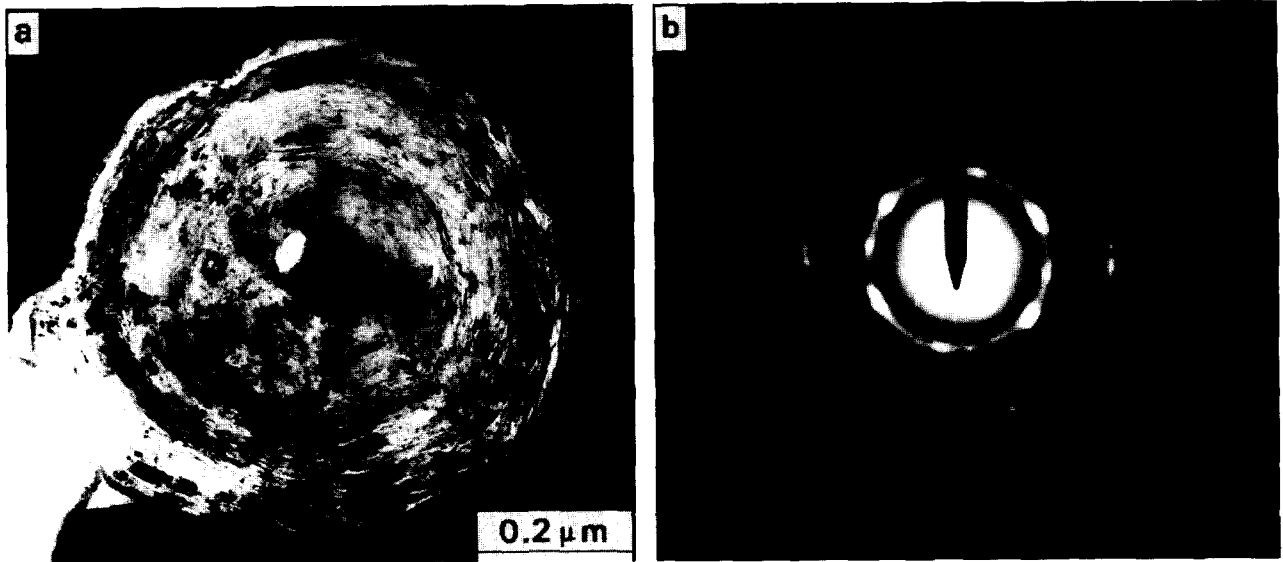


Fig. 5. (a) TEM image of a spherical graphite particle; (b) its diffraction pattern.

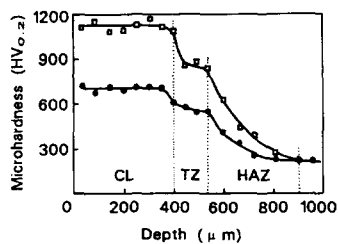


Fig. 6. Microhardness distribution curves:  $\square$ , 10vol.%SiC-Ni alloy;  $\bullet$ , pure Ni alloy; CL, clad layer; TZ, transition zone; HAZ, heat-affected zone.

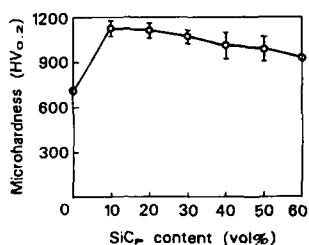


Fig. 7. Effect of  $\text{SiC}_p$  content on the microhardness of the clad layers.

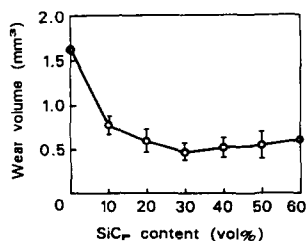


Fig. 8. Wear volume of the cladding vs.  $\text{SiC}_p$  content ( $P = 90 \text{ N}$ ;  $V = 1.47 \text{ mm s}^{-1}$ ;  $L = 180 \text{ m}$ ).

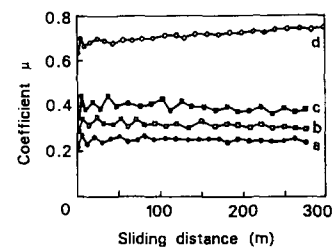


Fig. 9. Friction coefficient of the cladding ( $P = 90 \text{ N}$ ;  $V = 1.47 \text{ m s}^{-1}$ ): curve a, pure Ni alloy; curve b, 30vol.%SiC-Ni alloy; curve c, 10vol.%SiC-Ni alloy; and d, substrate.

significantly with increasing  $\text{SiC}_p$  content in the range 0–30 Vol.%, but no further decrease can be found with more than 30 vol.%  $\text{SiC}_p$ . Comparing Fig. 7 with Fig. 8, one can see that not only the microhardness but also the quantity of the precipitates within the clad layers determine the resulting wear resistance. If the volume fraction of the hard phases and their contiguity are too high so that the matrix is non-continuous, the wear resistance decreases from its highest value (e.g. the minimum wear volume).

The friction coefficient of the coatings is shown in Fig. 9, and it indicates a complex tendency with the addition of  $\text{SiC}_p$ . However, it is clear that the microhardness of the coatings associated with the  $\text{SiC}_p$  content has a substantial effect on the coefficient.

#### 4. Conclusions

(1) The complete dissolution of  $\text{SiC}_p$  occurred during laser melting and thus many carboborides

formed on solidification within the cladding. A microstructural evolution of the coatings was observed associated with the SiC<sub>p</sub> content.

(2) When the SiC<sub>p</sub> content was above 30 vol.%, silicides of Ni<sub>3</sub>Si<sub>2</sub> phase and graphite precipitates were found, and the  $\gamma$  matrix showed a tweed contrast anomaly.

(3) The addition of SiC<sub>p</sub> within the Ni alloy coatings led to a maximum increase in the microhardness by 410 HV and a maximum rise in the wear resistance to three times that of the SiC-free Ni alloy cladding.

## References

- [1] W. Cerri, R. Martinella et al., *Surf. Coat. Technol.*, **49** (1991) 40.
- [2] J.D. Ayers and R.N. Bolster, *Wear*, **93** (1989) 193.
- [3] Yu. Zuo and R.M. Latanision, *J. Mater. Sci.*, **27** (1992) 3014.
- [4] J.H. Abboud and D.R.F. West, *J. Mater. Sci. Lett.*, **10** (1991) 1149.
- [5] J.H. Abboud and D.R.F. West, *Mater. Sci. Technol.*, **5** (1989) 725.
- [6] G. Abbas, D.R.F. West, *Wear*, **143** (1991) 353.
- [7] B.H. Jiang and R. Wagner, *Acta Metal. Sinica*, **22** (1986) A500.